Electronic spectra and crystal field analysis of Yb^{2+} in $SrCl_2$

Zaifa Pan, Chang-kui Duan, and Peter A. Tanner*
Department of Biology and Chemistry, City University of Hong Kong, Tat Chee Avenue, Kowloon, Hong Kong SAR, People's Republic of China

(Received 21 July 2007; revised manuscript received 31 October 2007; published 19 February 2008)

The 10 K emission spectrum and absorption spectrum between 27 000 and 30 000 cm^{-1} have been recorded and assigned for $SrCl_2:Yb^{2+}$ (0.05 and 1 at. %), where the divalent ion is situated at a site of O_h symmetry with eightfold coordination to chloride ions. In emission, two broad bands are observed at room temperature and these are assigned to orbitally forbidden and allowed transitions from $4f^{13}5d$ to the $4f^{14}$ ground state $^1S_0$. Nearly all of the transitions, except for some of the highest energy absorption bands, are spin forbidden in the sense that the transition final states are dominated by spin triplet components, while the initial state is a pure spin singlet. The spectral intensities in the absorption spectrum have been fitted satisfactorily, following the crystal field calculation for $4f^{13}5d$ in which four parameters were freely varied. There is no need to cite the presence of Yb^{2+} ions at several sites in order to explain the observed absorption bands, as has been done previously, but we invoke the coparticipation of the (low-lying) $4f^{13}6s$ configuration. The rationale for the parameter values is explained in detail as are the effects of parameter variations. The calculated radiative lifetime for the orbitally allowed emission transition is in agreement with that measured at low temperature (~ 1 μs) and the nonradiative rate from the luminescent level has been modeled as a function of temperature.

DOI: 10.1103/PhysRevB.77.085114 PACS number(s): 78.55.−m, 33.70.−w, 32.30.Jc, 71.70.Ch

I. INTRODUCTION

Divalent rare earth ions doped into crystals have attracted attention because the electric dipole allowed transitions are at lower energies than in the corresponding trivalent ions so that strong ultraviolet or visible luminescence occurs. The clearly written review of Rubio O[1] has discussed the literature electronic spectra of Eu^{2+}, Sm^{2+}, and Yb^{2+} up to 1991. Much of this work has been carried out with high symmetry (cubic) host lattices comprising divalent cations, such as with group II metal halides, since the rare earth ion can directly substitute at one distinct crystallographic site without the requirement for charge compensation. These works have manifested not only applied scientific impact, but also theoretical repercussions. Early experimental studies of the optical spectra divalent rare earths enabled theories to be formulated concerning the selection rules for vibronic structure[2,3] and nonradiative transitions[4] as well as crystal field models.[5] Various theoretical approaches were employed in order to assign and interpret the energy levels derived from $4f^N \rightarrow 4f^{N-1}5d$ optical spectra. Piper *et al.* calculated the crystal field energy levels of Yb^{2+} in $SrCl_2$ (Ref. 6) in a *SLJM* scheme (*S, L, J, M,* being total spin, total orbit, total angular momenta, and projection quantum numbers, respectively), but a reinterpretation under a strong coupling scheme was later made by Loh.[7] Alig *et al.*[8] pointed out that the $5d$ electron exhibits a strong nephelauxetic effect so that considerable correction of the free ion parameters for fitting the energy levels of $4f^{N-1}5d$ is required. This correction was included in the calculations of Bland and Smith for $MX:Yb^{2+}$ (M=Na and K; X=F, Cl, Br, and I).[9]

Following the early, thorough studies of the spectra of Ln^{2+}, there has been an upsurge in interest during the present decade, particularly with regard to their phosphor properties,[10] and some of these publications are now mentioned. For Sm^{2+}, the effect of host lattice on the emission spectra,[11,12] luminescence quenching mechanisms,[13] and defect site symmetries[14] has been investigated. Divalent europium has been studied most widely, and this ion is particularly stable in structures with rigid networks of AO_4 groups[15] (A=B and P) and in glasses.[16] Applied studies have investigated the properties of Eu^{2+} in the $SrLaGa_3S_6O$ phosphor[17] and the synthesis of $SrAl_2O_4:Eu^{2+}$ nanocrystals.[18] Theoretically, the two photon transition intensities[19] and the unusual temperature dependence of the Eu^{2+} lifetime in CaF_2 crystals have been modeled.[20] The optical spectra of $SrCl_2:Eu^{2+}$ have recently been reinvestigated and simulated by calculation.[21] The participation of conduction band states in the thermal quenching of the interconfigurational luminescence of Eu^{2+} (Refs. 22 and 23) as well as the location of the $4f^6 5d \rightarrow 4f^7$ transition in various Eu^{2+} doped materials[24] and its relationship with the corresponding energy for Ce^{3+}[25] have been investigated. The relationship between the coordination environment of Eu^{2+} and the crystal field splitting of $4f^6 5d$ energy levels was clarified by Dorenbos.[26] It was found that the crystal field splitting decreases with increasing size of the coordination polyhedron and the dependence on the average distance to the ligands was found to be R^{-2}. Recent studies of the luminescence spectra of Tm^{2+} have focused on the upconversion luminescence,[27] the effects of chemical variation on emission spectra,[28] and the observations of $4f$-$4f$ and $5d$-$4f$ emissions.[29] The coexistence of Yb^{3+} together with Yb^{2+} in crystals has been recognized as problematic for the interpretation of optical spectra.[7,30,31] Emission spectra of Yb^{2+} have been reported in many crystals, such as MgF_2,[32] CaF_2,[33,34] $YAlO_3$,[35] $Y_3Al_5O_{12}$,[35] $LiBaF_3$,[35] $LiCaAlF_6$,[36] MSO_4 (M=Ca, Sr, and Ba),[37] $AYbI_3$ (A=K, Rb, and Cs),[38] and $NaCl:(CN^-)_x$,[39] and the quenching in certain lattices has been investigated.[40,41] As recognized for the second half of the series of trivalent lanthanides, the luminescent state in $4f^{N-1}5d \rightarrow 4f^N$ transitions of the relevant divalent ions can be of high spin or low spin character depending on the spin

coupling of the $5d$ electron with the $4f^{N-1}$ core.[42] We recently pointed out that the energy separation of "low-spin" and "high-spin" states cannot be made by inspection of spectral data but requires calculation, because most $4f^{N-1}5d$ states are of mixed spin parentage.[43] Empirical correlations concerning the "spin-allowed" and "spin-forbidden" transitions have been presented for Yb^{2+}.[41,44] Indeed, it has become common practice to label the lowest states of Yb^{2+} as high spin and low spin.[45] We show herein, as noted in an early study,[6] that the distinction of these states is rather based on orbital symmetry than spin composition since all of the lower states are predominantly high spin.

Our present investigations focus on Yb^{2+} doped into $SrCl_2$ since there are no charge compensation requirements when substituting Yb^{2+}(VIII) with ionic radius of 1.14 Å for Sr^{2+}(VIII) with ionic radius of 1.26 Å in this host lattice. As mentioned above, the interpretation of the absorption spectra has been made by various different approaches and requires clarification. The reported luminescence spectra comprised five bands which exhibited a complex behavior with temperature.[31] Therefore, in this study, we have made experimental reinvestigations of the low energy absorption spectrum and of the luminescence and decay kinetics of $SrCl_2:Yb^{2+}$, and provided detailed theoretical interpretations of the results. It is necessary to draw upon previous spectral results for the $SrCl_2:Yb^{2+}$ system which were carried out at lower temperatures, under compression or using polarized radiation under the application of a magnetic field, in order to guide us to our conclusions. Following a brief description of the experimental setup (Sec. II), the electronic absorption spectrum is described in Sec. III A with reference to the optical properties which have previously been reported for Yb^{2+} diluted in cubic $SrCl_2$. The discussion of the emission spectra (Sec. III B) is followed by the rationale employed in the energy level calculations and the ensuing results (Sec. III C). Radiative emission lifetimes, nonradiative processes, and emission intensity ratios are discussed in Sec. III D via the application of the energy calculation results. Finally, the main conclusions are listed in Sec. IV.

II. EXPERIMENT

Samples of $SrCl_2$ doped with Yb^{2+} at nominal atomic concentrations of 0.05% and 1% were prepared by a solid-state reaction with the starting materials of $SrCl_2$, Yb metal, and Yb_2O_3 in stoichiometric quantities. Yb_2O_3 (Strem Chemicals, 99.9% or 99.999%) was dissolved in hot concentrated hydrochloric acid (37%, Riedel-de Haën, RG) and, after a clear solution was obtained, $SrCl_2$ (Aldrich Chemicals, 99.995%) was added stoichiometrically. After dissolution, Yb metal (Aldrich Chemicals, 99.9%) was added, and it quickly dissolved. The resulting solution was then evaporated to dryness and the solid obtained was powdered under strong heating in order to exclude moisture and then transferred to a clean, preheated quartz tube. The tube was heated under vacuum inside a furnace at 673 K for two days prior to sealing off as an ampoule. The ampoule was lowered through a Bridgman furnace at 1173 K at a rate of 1.2 cm h^{-1}. Further manipulations were carried out in a dry box under a nitrogen atmosphere, where the boule was broken and, after polishing, the crystal was sealed inside an adhesive coating. Samples of doubly doped $SrCl_2:Yb^{2+}$, Eu^{2+} were also prepared in a similar manner. Attempts to prepare $SrCl_2:Yb^{2+}$ by carbon reduction of Yb^{3+} (without the use of the lower-purity Yb metal) failed. The Yb_2O_3 starting material was found to contain 40 ppb Eu on analysis by inductively coupled plasma mass spectroscopy.

Emission spectra were recorded at room temperature using a Jobin Yvon Fluoromax-3 spectrofluorometer with the slit set at 3 nm. Higher resolution ($2-4$ cm^{-1}) emission spectra were recorded from room temperature to 10 K using the 355 nm line of a Surelite Nd:YAG (where YAG denotes yttrium aluminum garnet) laser. The crystals were mounted in an Oxford Instruments closed cycle cryostat. The emission was collected at 90° and passed through an Acton 0.5 m monochromator equipped with a SpectruMM charge-coupled device. Alternatively, a Hamamatsu R928 photomultiplier tube was used as detector, in particular, with a Tektronix TDS 5054B 500 MHz digital oscilloscope to record the emission decay. The uncertainty of the measured lifetimes from the curve fitting was in the range of 1%–3% and the lifetime varied by 1%–4% for different sections of the emission peak. For temperatures <50 K, the uncertainty in lifetime was up to 10%.

Electronic absorption spectra were recorded using the same monochromator with a Xe or D_2 lamp light source. Absorption spectra in the infrared region showed the presence of Yb^{3+} in our crystals.

III. RESULTS AND DISCUSSION

A. Absorption spectrum of $SrCl_2:Yb^{2+}$

The ion Yb^{2+} possesses the $4f^{14}$ configuration with a $^1S_0$ ground state multiplet term. The first excited state belongs to the $4f^{13}5d^1$ configuration. Since the Yb^{2+} ion occupies a site of cubic symmetry in the $SrCl_2$ host, the irreducible representations of the orbital wave functions of electronic states are conveniently expressed in the O_h molecular point group. Absorption transitions from the A_{1g} ground state are only electric dipole allowed to the (18) terminal T_{1u} states. Figure 1 shows the lowest energy groups of bands in the 10 K electronic absorption spectrum of $SrCl_2:Yb^{2+}$. The position of the lowest energy electronic origin is confused by the superposition of emission bands at lower energy, which appear as "dips" (not shown in Fig. 1), and it is located more clearly in the 4.2 K spectrum of a crystal containing less than 0.06 at. % Yb^{2+} shown in Fig. 5 of Piper *et al.*[6] Two electronic origins are thus located at (± 5 cm^{-1}) 27 049 and 29 049 cm^{-1} in Fig. 1, with the latter being much weaker, and are assigned to transitions to terminal T_{1u} states. Based on each zero phonon line, there are vibrational progressions in a mode of 213 ± 3 cm^{-1}, indicated by vertical bars in Fig. 1, with additional strong vibronic structure at 114 ± 2 cm^{-1}. This energy is similar to those in the absorption spectra of $SrCl_2$ doped with Tm^{2+} (Ref. 8) and Sm^{2+}.[4] The lattice dynamics calculation of crystalline $SrCl_2$ indicates transverse and longitudinal optic modes at 155 and 248 cm^{-1}, respectively.[46] Wagner and Bron assigned a similar structure

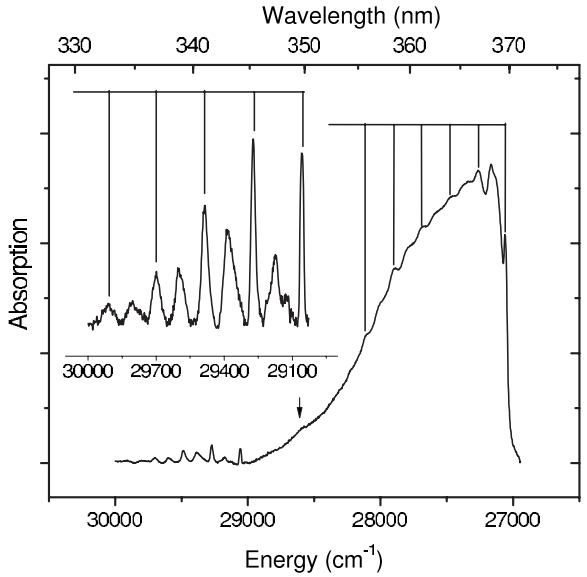

FIG. 1. Lowest energy groups of bands between 330 and 380 nm in the 10 K Xe-lamp absorption spectrum of $SrCl_2:Yb^{2+}$ (1 at. %).

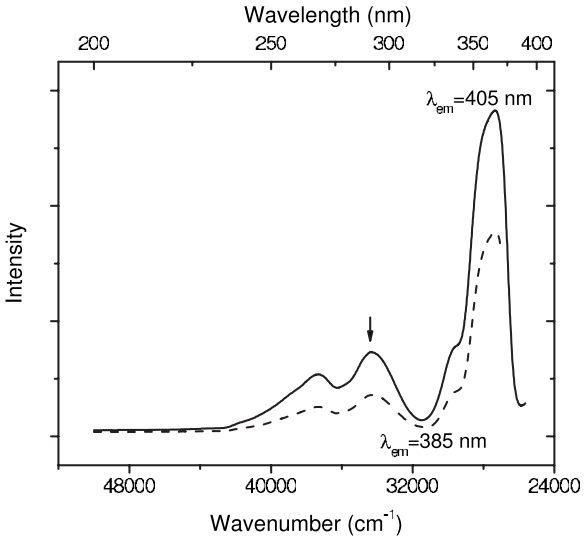

FIG. 2. Room temperature excitation spectra of $SrCl_2:Yb^{2+}$ (0.05 at. %) monitoring the emission at 405 nm (solid line) and 385 nm (dashed line).

in the absorption spectra of rare earth divalent ions doped in alkali halide crystals to pseudolocalized vibrations.[3] Indeed, the structure is even similar to the electric dipole allowed transitions of trivalent lanthanides in elpasolite lattices, where structure was assigned to totally symmetric Ln^{3+} vibrations with successively distant shells of neighbors.[47] The results in Fig. 1 are, thus, in agreement with the spectra of Piper *et al.*[6] except that we tentatively notice in our more concentrated samples a further broad structure (labeled by an arrow in Fig. 1 and centered at 28 590 cm^{-1}) which is not associated with the first transition and presumably corresponds to a very weak transition involving the first member of the 213 cm^{-1} progression of another T_{1u} state. The room temperature excitation spectra of emission bands at 405 nm (24 690 cm^{-1}) and 385 nm (25 975 cm^{-1}) are shown in Fig. 2. The peaks correspond to analogous features in the room temperature absorption spectrum of Piper *et al.*,[6] but the feature at 292 nm (34 250 cm^{-1}; marked by an arrow) is due to the adhesive used to coat the crystal.

B. Emission spectrum of $SrCl_2:Yb^{2+}$

Several previous studies have reported the emission spectrum of $SrCl_2:Yb^{2+}$. Witzke *et al.*[31] reported five bands between 17 000 and 27 000 cm^{-1} and labeled them I–V. We identify some of these bands (III, IV, and V) as impurity species since we do not observe them. The evolution of bands I and II from 170 K to room temperature, under 355 nm excitation, is shown in Fig. 3 for a sample of 0.05 at. % Yb^{2+} in $SrCl_2$. At room temperature, the bands labeled I and II are of similar intensity, but band II rapidly decreases in intensity below about 230 K. Band II is associated with a forbidden transition under O_h site selection rules, and the temperature dependence is discussed in Sec. III D. Basically, the luminescent states of band II are populated by nonradiative relaxation from the upper emission level and the rate is very slow at low temperatures. The emission spectrum at about 10 K is shown in Fig. 4(a). The zero phonon line of the high energy band is coincident, within the accuracy of our measurements, with that in the absorption spectrum. This band was assigned to a $T_{1u} \rightarrow A_{1g}$ transition from the lowest T_{1u} state by Witzke *et al.*,[31,48] and this was confirmed in other studies by careful measurements under the application of uniaxial pressure[49] and the measurements using a magnetic field.[50,51] Indeed, the band structure is similar to that in the absorption spectrum as well as to other electric dipole allowed transitions of divalent rare earth ions. The vibrational progression frequency for band I is 209 ± 2 cm^{-1} (literature:[51] 210 cm^{-1}), showing that a slight bond length contraction occurs in the $4f^{13}5d$ state compared with the electronic ground state, measured from Franck-Condon

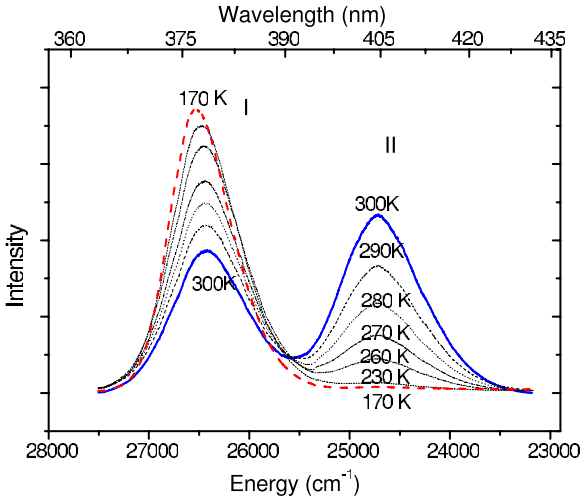

FIG. 3. (Color online) Evolution of the 355 nm excited emission spectrum of $SrCl_2:Yb^{2+}$ (0.05 at. %) between room temperature and 170 K.

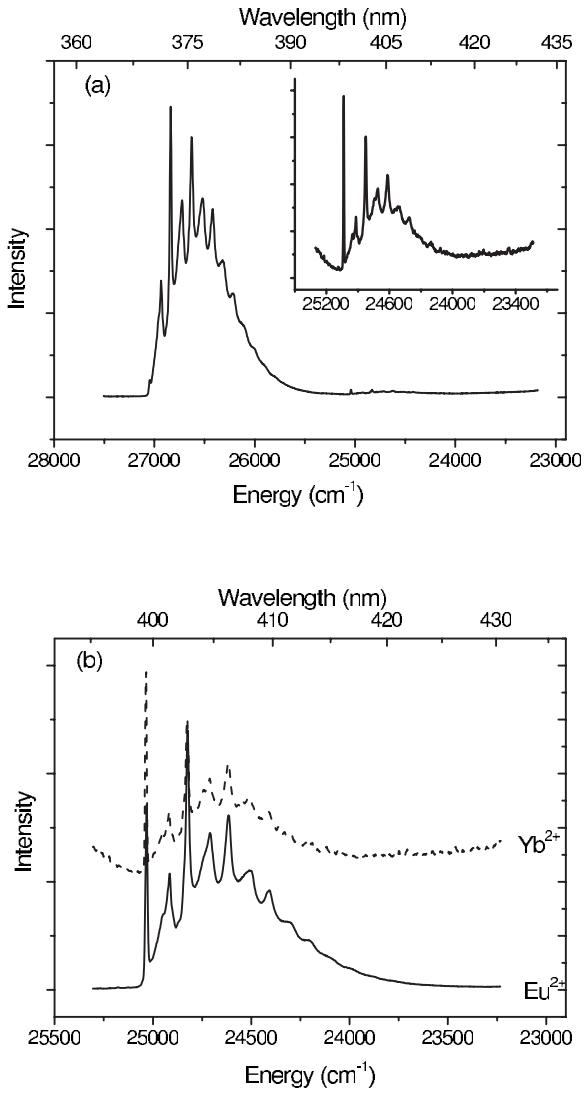

FIG. 4. (a) 355 nm excited 10 K emission spectrum of $SrCl_2:Yb^{2+}$ (0.05 at. %) between 360 and 425 nm. The inset shows an ordinate expansion to longer wavelengths than 397 nm. (b) Detailed comparison of the lower energy band in (a) with the emission spectrum of $SrCl_2:Eu^{2+}$.

analysis[52] to be 3.8 pm, compared with the same value derived from the absorption spectrum. Another vibronic structure is identified at 85, 114, and 131 cm^{-1} below the zero phonon line. The emission spectrum is similar for the 0.05 and 1 at. % Yb^{2+} samples although the former spectrum is more clearly resolved.

Measurements in other studies at 2 K have shown that emission occurs from a T_{2u} level at 7 cm^{-1} below the T_{1u} state.[49–51] The zero phonon line is absent from this emission and the vibronic structure differs from that of $T_{1u} \rightarrow A_{1g}$, with frequencies of 85, 191, and 212 cm^{-1}. Turning to the weak, lower energy emission in Fig. 4(a), the comparison made in Fig. 4(b) of this emission band with the emission spectrum of $SrCl_2:Eu^{2+}$ (Ref. 21) shows that the spectra are effectively identical. The structure is typical of an electric dipole allowed transition, with the zero phonon line at 25 044 cm^{-1}. On codoping $SrCl_2$ with 0.1 at.% Eu and 0.1 at. % Yb, the Yb^{2+} emission was absent even at room temperature, whereas Eu^{2+} emission was observed. Therefore, the lower energy emission band at low temperature in our work (Fig. 4) is due to Eu^{2+}. Not only is Eu^{2+} directly excited by 355 nm radiation, but also energy transfer occurs from Yb^{2+} to the minute amount of Eu^{2+} in the crystal since there is an efficient spectral overlap of Yb^{2+} emission and Eu^{2+} absorption. Unfortunately, we were unsuccessful in preparing $SrCl_2:Yb^{2+}$ by carbon reduction of the high purity (99.999%) oxide Yb_2O_3, following the same procedure that we used for $SrCl_2:Eu^{2+}$.

Witzke *et al.*[31] observed a lower energy emission band below 24 958 cm^{-1} in $SrCl_2:Yb^{2+}$ and very weak absorption bands above about 25 088 cm^{-1} (Fig. 3 of Ref. 31). These bands are not due to Eu^{2+} and they were assigned to (vibronic structure of) orbitally forbidden transitions involving A_{1g}-T_{2u}, E_u states. Here, by the terms *orbitally forbidden* or *allowed*, we mean that the selection rule is based on the point group irreducible representation of the orbitals (wave functions) of the involved states. The electronic origin is not expected to be observed for these transitions and the assignments of bands are ambiguous, particularly since new vibronic structure is observed at about 410 cm^{-1} below the first emission band at 24 958 cm^{-1}. The progression frequency is rather higher (about 215 cm^{-1}) for the emission bands compared with the corresponding weak absorption bands (about 204 cm^{-1}) (Fig. 3 of Ref. 31). The exact location of the lowest energy $4f^{13}5d$ state cannot be clearly made, but it is certainly between 24 958 and 25 075 cm^{-1}. Note that the value 25 252 cm^{-1} given in Table I is taken from the extrapolation to 10 K of the separation between the two maxima in the room temperature emission spectrum, Fig. 3 of our work. This value does not refer to the location of an electronic origin, but to the band maximum.

C. Energy level calculations for Yb^{2+} in $SrCl_2$

1. Results of energy level fitting

The $4f^{13}5d$ configuration of Yb^{2+} comprises the terms[1,3] (PDFGH) of total degeneracy 140, which give the ungerade irreducible representations $6A_1+5A_2+12E+18T_1+17T_2$ in the O_h molecular symmetry point group. The certain location of only two electronic energy levels (T_{1u}: 27 049 cm^{-1}, T_{2u}: 27 042 cm^{-1}) can be made from the emission spectra, with a further one (T_{1u}: 29 049 cm^{-1}) in absorption. In order to perform the energy level fitting, we therefore utilize the reported absorption spectrum of $SrCl_2:Yb^{2+}$ at 4.2 K of Piper *et al.*[6] from 190 to 380 nm, which permits the location of 12 of the 18 T_{1u} states. These assignments refer to the *peak intensity* of each transition, because only a broad, unresolved structure is observed, and not to the zero phonon line energy so that all levels are effectively shifted up by ~210 cm^{-1} from the zero phonon line energies. This does not affect the important parameters in our calculations because the $4f^{13}5d$ levels are shifted arbitrarily by the barycentre energy E_{exc}. We have also included the assignments deduced in Sec. III B for the lowest $4f^{13}5d$ level, and the T_{2u} level, and corrected these zero phonon line energies for (hypothetical) band centers so that 14 experimental energy levels can be fitted.

TABLE I. Energy levels of the $4f^{13}5d$ configuration for $SrCl_2:Yb^{2+}$. Experimental energy levels and intensities are taken from Piper *et al.* (Ref. 6). Theoretical energy levels and intensities are calculated with the optimized parameters presented in Table II.

		First component			Energy			Intensity		
No.	Irrep[a]	^{2S+1}L	J	M	E_{calc}[b]	E_{expt}[c]	ΔE[d]	Calc. DS[e]	Calc. ROS[f]	Expt. ROS[a]
1	E_u	^3P	2	0	25303	25252	51			
2	T_{2u}	^3P	2	1	25307					
3	T_{2u}	^3D	3	1	27227	27255	−28			
4	T_{1u}	^3H	5	5	27234	27262	−28	79.2	1	1
5	A_{2u}	^3D	3	−2	27276					
6	E_u	^1D	2	0	27453					
7	T_{1u}	^3D	3	−3	27572			11.1	0.14	
8	T_{2u}	^3D	3	1	27586					
9	A_{1u}	^3F	4	0	28066					
10	T_{1u}	^3F	4	1	28154	(28590)		3.18	0.04	
11	E_u	^3G	5	−4	29110					
12	T_{1u}	^3F	3	0	29293	29272	21	1.92	0.03	0.04
13	T_{2u}	^1G	4	−3	29478					
14	E_u	^3H	6	0	35082					
15	T_{2u}	^3H	6	1	35100					
						(35028)[h]				0.15 (0.13)
16	T_{1u}	^3P	1	1	35594			1.47	0.02	
17	A_{1u}	^3P	0	0	35616					
18	T_{2u}	^3H	6	5	36773					
19	E_u	^1D	2	2	36796					
20	T_{1u}	^3H	6	−3	36932			0.05	0.0008	
21	A_{2u}	^3H	6	−2	36935					
22	T_{2u}	^1D	2	1	36978					
23	E_u	^3H	4	2	37194					
24	T_{1u}	^3H	4	1	37208	37219	−25	0.55	0.009	0.07 (0.16)
25	A_{1u}	^3H	6	4	37237					
26	T_{1u}	^3D	3	−3	37510	37625	−115	2.1	0.04	0.1 (0.20)
27	T_{2u}	^3D	2	1	37763					
28	T_{2u}	^3F	4	−3	37991					
29	T_{2u}	^3H	4	3	38156					
30	E_u	^3F	2	0	38323					
31	T_{1u}	^3G	5	4	38559			8.38	0.15	
32	E_u	^3G	5	−4	38732					
33	T_{1u}	^3H	5	0	38975	38748	227	114	2.1	1.9 (1.1)
34	T_{1u}	^1F	3	0	39149			48.1	0.87	
35	E_u	^1D	2	0	39485					
36	A_{1u}	^1G	4	0	39546					
37	A_{2u}	^3G	3	2	39734					
38	T_{1u}	^1F	3	0	39782	39749	33	38.1	0.70	0.59 (1.1)
39	T_{2u}	^1G	4	−3	39785					
40	T_{2u}	^3G	5	5	39848					
41	T_{2u}	^3G	4	−3	40080					
42	A_{2u}	^3G	3	2	40361					
43	T_{1u}	^3G	5	5	41175	41089	86	332	6.3	3.4 (2.4)
44	A_{1u}	^3P	0	0	45045					

TABLE I. (*Continued.*)

		First component			Energy			Intensity		
No.	Irrep[a]	^{2S+1}L	J	M	E_{calc}[b]	E_{expt}[c]	ΔE[d]	Calc. DS[e]	Calc. ROS[f]	Expt. ROS[a]
						45794[h]				(0.2)
45	T_{1u}	^3D	1	1	46712	46649	63	50.2	1.1	1.1 (0.4)
46	E_u	^3F	2	0	47050					
47	T_{2u}	^3H	4	−3	47259					
48	T_{2u}	^1D	2	1	47498					
49	E_u	^3D	2	0	47594					
50	T_{1u}	^3H	5	−3	48251			80.8	1.8	
51	T_{1u}	^1P	1	1	48533	48575	−42	494	11.1	4.4 (2.8)
52	T_{2u}	^3G	3	1	49087					
53	A_{2u}	^1F	3	−2	49264					
54	T_{1u}	^3G	3	−3	49766			0.02	0.0004	
55	T_{2u}	^3F	2	1	49826					
56	E_u	^3G	4	0	50051					
57	T_{1u}	^3G	4	1	50390	50403	−13	13.8	0.32	1.2 (1.8)
58	A_{1u}	^3G	4	0	50471					

[a]Irrep is the O_h molecular point group irreducible representation of the state.
[b]E_{calc} are calculated energies of the states shifted relative to the peak position in absorption spectra; refer to the text.
[c]E_{expt} are measured energies of the states shifted relative to the peak position in absorption spectra; refer to the text.
[d]$\Delta E = E_{calc} - E_{expt}$; the standard error for the fitting to $N_{expt}=12$ levels with $N_{param}=4$ parameters is $\sigma = \sqrt{\Sigma_i \Delta E_i^2/(N_{expt}-N_{param})} = 103$.
[e]Calc. DS is the calculated dipole strength in unit of 10^{-20} cm^2.
[f]Calc. ROS is calculated (proportional to product of Calc. DS and E_{calc}) relative oscillator strength.
[g]Expt. ROS is experimental (Ref. 6) relative oscillator strength. We have remeasured the relative oscillator strengths after baseline subtraction and these values are in parentheses.
[h]These levels are assigned to the $4f^{13}6s^1$ configuration.

Table I compares the $4f^{13}5d$ level energies with the calculated values using the Reid suite of *fd* shell programs,[53,54] and the rationale for the choice of parameters is now explained. Indeed, our calculations went through several revisions until the optimized values were attained. The final energy parameters are listed in Table II and are compared with those of Piper *et al.*[6] The detailed description of these parameters and of the energy level fitting process have been given elsewhere[53,54] and is not repeated here. The parameters were optimized by minimizing the root mean square (rms) of the differences between the calculated and measured 12 energies listed in Table I. Parameters in square brackets were fixed. The ratios of the atomic *fd* interaction parameters $G^3(fd)/G^1(fd)$ and $G^5(fd)/G^1(fd)$ were held at the ratios of the free ion values 7755/6762 and 6266/6762, respectively. The fitted value of $G^1(fd)$ is 0.694 times the Yb^{2+} free ion value of 6762 cm^{-1}, which is due to delocalization of the $5d$ electron over the ligands.[54] The $F^4(fd)/F^2(fd)$ ratio was held at the *ab initio* ratio of 9868/19614 and the fitted $F^2(fd)$ value turned out to be 0.732 times the free ion value. The free ion values $\zeta(ff)=2950$ cm^{-1} and $\zeta(dd)=1211$ cm^{-1} were used for the $4f$- and $5d$-electron spin-orbit coupling constants. The $4f$-electron crystal field parameters were constrained to appropriate values. $B_0^4(ff)$ was assigned 0.7 times the value for $SrCl_2:Eu^{2+}$,[21] since this is the ratio of $B_0^4(ff)$ $(Cs_2NaYbCl_6)/B_0^4(ff)$ $(Cs_2NaEuCl_6)$. The sixth-degree crys-

TABLE II. Parameter values used for the energy level calculations.

Parameter[a]	Value (cm^{-1})	Value converted from those in Ref. 6 (cm^{-1})
E_{exc}	38382	[F^0=44073]
$B_0^4(dd)$	−20442	−16800
$\zeta(ff)$	[2950]	2950
$F^2(fd)$	14355	19614
$F^4(fd)$	[7222]	9868
$G^1(fd)$	4693	6762
$G^3(fd)$	[5382]	7755
$G^5(fd)$	[4349]	6266
$\zeta(dd)$	[1211]	1211
$B_0^4(ff)$	[−725.0]	−1450
$B_0^6(ff)$	[292][b]	560

[a]The energy level parameters E_{exc}, $B_0^4(dd)$, $F^2(fd)$, and $G^1(fd)$ were optimized by minimizing the root mean square of the differences between the calculated and measured 12 energies both listed in Table I. Parameter values in square brackets were held fixed as rationalized in the text.
[b]$B_0^6(ff)$ is adjusted after the optimization to reflect the definite splitting of 7 cm^{-1} between the first T_{1u} (No. 4 in Table I) and the underlying T_{2u} (No. 3 in Table I).

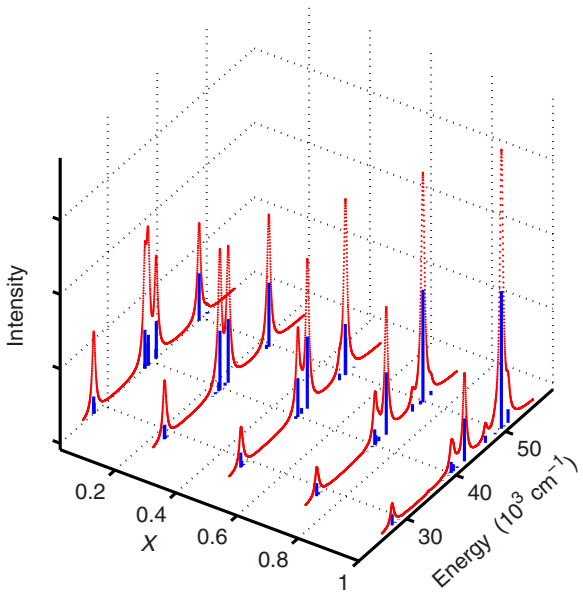

FIG. 5. (Color online) Calculated absorption spectra of $SrCl_2:Yb^{2+}$ as a function of the scaling factor for $4f5d$ Coulomb interaction parameters in the range $0 \leqslant x \leqslant 1$ ($x=1$ being the free ion case).

tal field parameter $B_0^6(ff)$ was originally fixed by the ratio $B_0^6(ff)/B_0^4(ff)=-0.2$,[9] which was extrapolated from the values of −0.18 for $CaF_2:Ho^{2+}$ (Ref. 55) and −0.19 for $CaF_2:Tm^{2+}$.[56] Actually, our calculations show that changes of the values of $B_0^4(ff)$ and $B_0^6(ff)$ have only minor effects on the calculated absorption spectra. Actually, the value of $B_0^6(ff)$ for $SrCl_2:Eu^{2+}$ was taken to be negative[21] since the energy levels were relatively insensitive to this fitting parameter, but a point charge model predicts a positive value, as in several other systems. For example, the values of the $4f$ crystal field parameters fitted by Alig *et al.*[8] for $SrCl_2:Tm^{2+}$ were (in cm^{-1}) $B_0^4(ff)=-464$ cm^{-1} and $B_0^6(ff)=416$ cm^{-1}. The remaining parameters E_{exc}, the barycenter of the $4f^{13}5d$ configuration, and $B_0^4(dd)$ were fitted. The parameter $B_0^4(dd)$ is equivalent to $21Dq$ or $2.1[E(5d\ e_g)-E(5d\ t_{2g})]$. Thus, in total, four energy parameters were varied in the initial energy level calculations. Finally, the parameter $B_0^6(ff)$ was further optimized to get the accurate splitting of 7 cm^{-1} between the lowest T_{1u} and the underlying T_{2u}. The effect of this final optimization changing $B_0^6(ff)$ from the fixed value of 145 to 292 cm^{-1} on other levels is much less than their experimental uncertainty. Other criteria besides the locations of energy levels are important when performing the energy level fitting, and we particularly take into account the fitting of spectral intensities and the modeling of g factors. As Piper *et al.*[6] pointed out, the only allowed transitions in absorption are those to terminal T_{1u} states which comprise some $^1P_1$ parentage.

2. Effects of variation of energy parameters

This section discusses in some detail how the energy parameters are constrained by experimental data. Figure 5 shows the evolution of the absorption spectrum of $SrCl_2:Yb^{2+}$ as a function of the scaling factor x, between 0 and 1, for fd Coulomb interaction parameters compared with the free ion values, when other parameters are held at the constant values in Table II. The value of E_{exc} was adjusted (it was reduced with increasing x) to keep the barycenter of the calculated and measured levels at the same position. In the case $x \sim 0$, the absorption spectrum is composed of four groups of bands, derived from two bands from the spin-orbit splitting of the $4f$ orbitals, times two for the crystal field splitting of the $5d$ orbitals. The almost-equal $4f$-spin-orbit and $5d$-crystal-field splittings lead to the overlap of the two middle groups. With increasing interactions x, the two overlapping middle groups mix and split further apart into two new groups. One group moves downward to the 35 000–39 000 cm^{-1} region and has dominant high-spin components and, therefore, the absorption dipole strength from $4f^{14}(^1S_0)$ is very small. This group is not noticeable in the figure. The other group of bands has dominant low-spin components and large absorption dipole strength, and it moves slightly upward to the 39 000–41 000 cm^{-1} region. The strong $x \sim 0$ peaks at ~27 000 and ~48 000 cm^{-1} lose and gain intensities, respectively, with increasing x. Since the $4f$-spin-orbit interaction and the $5d$-crystal-field interaction do not commute with the fd Coulomb interaction, some states with dominantly high-spin components may mix small amounts of low-spin components containing $^1P_1$ and can be observed as weak absorption peaks. Further calculations show that the changing pattern of the calculated absorption spectra is mainly due to the Coulomb interaction $F^k(fd)$ ($k=2$ and 4) and $G^k(fd)$ ($k=1$, 3, and 5) parameters, and this constrains the value of those parameters greatly in the fitting. With very strong interaction between the $4f$ and $5d$ electrons ($x \gg 1$), the absorption spectrum intensifies toward the level dominated by $^1P_1$ in the group with the highest energy, thus approaching the Yb^{2+} free ion case, where x is actually 1 but, since $B_0^4(dd)=0$, the effect of fd Coulomb interaction is dominant.

We now consider the energy and intensity dependence of the group of levels at lowest energies (<27 000 cm^{-1}) on the other parameters. In Sec. III B, the photoluminescence spectra showed that there are two sets of emissive levels, with band I at ~27 000 cm^{-1} (observable in absorption) and the other at ~25 000 cm^{-1} (band II; not readily observable in the absorption spectra). First, we examine changes on the variation of $4f$-electron crystal field parameters while keeping other parameters fixed at the values in Table II. As shown in Fig. 6, with $\Delta B_0^4(ff)=B_0^4(ff)-(-725)$ cm^{-1} changing from 500 to −500 cm^{-1}, the upward moving T_{1u} level (No. 4 in the figure, associated with strong absorption) approaches the downward moving T_{1u} level (No. 7 in the figure, associated with weak absorption) and then splits off as $B_0^4(ff)$ becomes more negative. Our initial calculation[57] assigned the lowest T_{1u} level to the lowest room temperature emission band II at 25 252 cm^{-1}, with the second lowest T_{1u} level to the 27 262 cm^{-1} band I. Together with the fitting of other experimental levels, the optimized value of $B_0^4(ff)$ was −6500 cm^{-1}, which is more than twice the magnitude of $B_0^4(ff)$ for the $4f^7$ configuration of Eu^{2+} in CaF_2 (Ref. 58) and substantially too large. We, therefore, discarded the as-

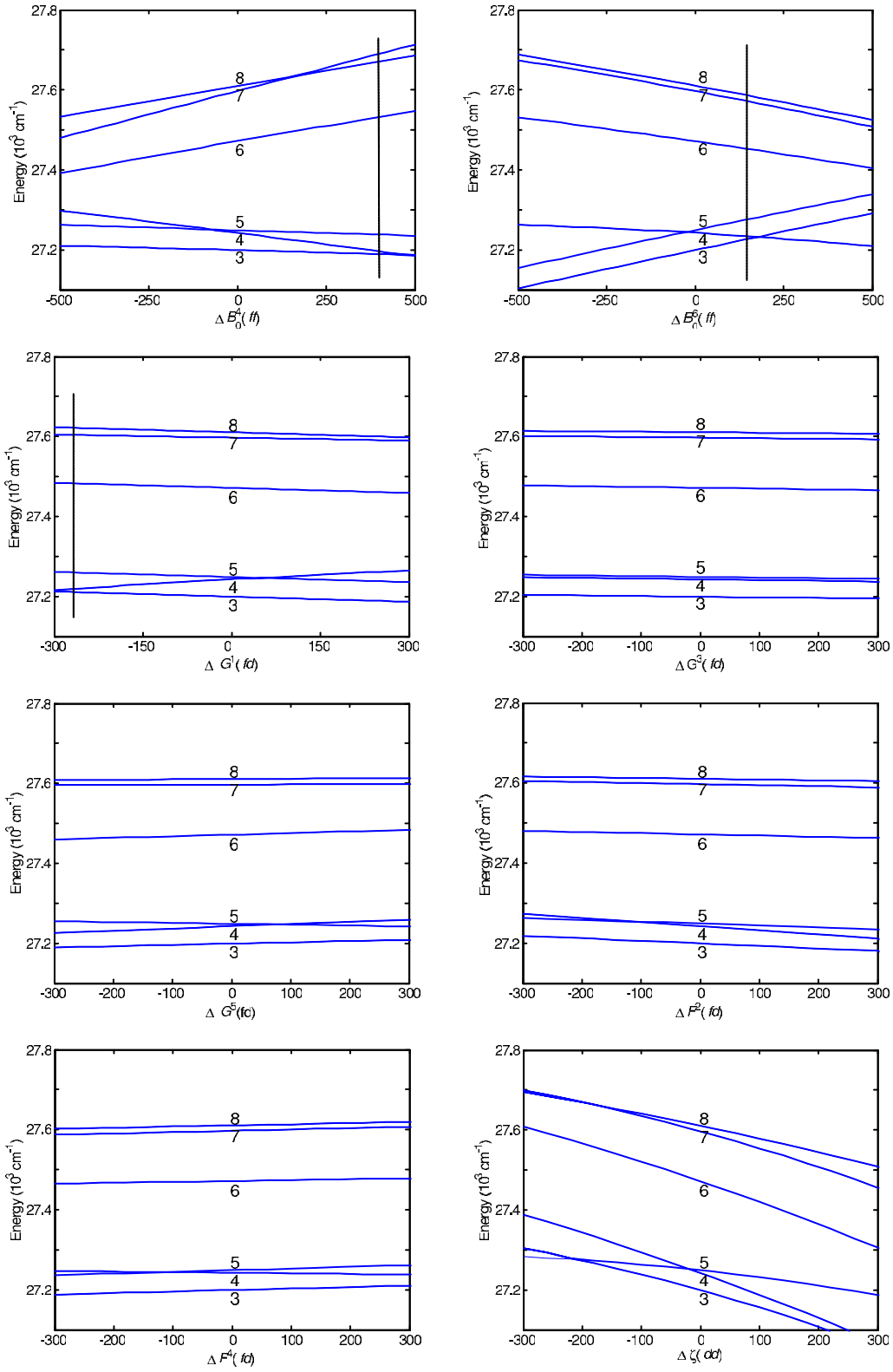

FIG. 6. (Color online)Variation of the energy levels near the lowest T_{1u} emission level of $SrCl_2:Yb^{2+}$ with deviations of parameters. Only one parameter is varied at a time, and all other parameters are fixed at the values in Table II, except $B_0^6(ff)$, which is fixed at 145 cm^{-1}.

signment of the lowest energy emission to a T_{1u} state and adopted the value of −725 cm^{-1} for $B_0^4(ff)$, being scaled phenomenologically from the value in $SrCl_2:Eu^{2+}$. Figure 6 also shows that with $\Delta B_0^6(ff)=B_0^6(ff)-145$ cm^{-1} changing from −500 to 500 cm^{-1}, the lowest upwardly moving level is T_{1u} (No. 4) and the next upwardly moving level is A_{2u} (No. 5). The T_{2u} level (No. 3) has a fairly flat variation with $\Delta B_0^6(ff)$. The increase within a factor of 2 (not fully shown in Fig. 6)

TABLE III. $^{2S+1}L_J$ composition of components of certain calculated energy levels with >5% parentage.

No.	Energy (cm^{-1})	Components with >5% in weight
1	25303	$^3P_2(55\%)+{}^3H_6(30\%)+{}^3D_2(7\%)$
2	25307	$^3P_2(54\%)+{}^3H_6(26\%)+{}^3D_2(6\%)$
3	27227	$^3H_5(22\%)+{}^1H_5(18\%)+{}^3H_6(16\%)+{}^3D_3(16\%)+{}^1D_2(10\%)+{}^3D_2(6\%)$
4	27234	$^3H_5(36\%)+{}^1H_5(29\%)+{}^3P_1(12\%)+{}^3D_1(10\%)$
5	27276	$^3H_6(44\%)+{}^3D_3(40\%)+{}^3F_3(14\%)$
6	27453	$^3H_5\ 26\%)+{}^1H_5(22\%)+{}^1D_2(14\%)+{}^1G_4(10\%)+{}^3D_2(8\%)+{}^3F_4\ 7\%)$
7	27572	$^3D_3(25\%)+{}^3H_5(18\%)+{}^3H_6(16\%)+{}^3G_5(13\%)+{}^1H_5(8\%)+{}^3G_4(6\%)$
8	27586	$^3H_6(22\%)+{}^3D_3(18\%)+{}^3F_3(12\%)+{}^1H_5(10\%)+{}^1D_2(8\%)+{}^3H_5(6\%)+{}^3G_5(6\%)+{}^3D_2(6\%)$
33	38975	$^3H_5(22\%)+{}^1G_4(22\%)+{}^3G_5(15\%)+{}^3F_4(14\%)+{}^1P_1(9\%)+{}^3F_3(5\%)$
38	39782	$^1F_3(25\%)+{}^3G_4(18\%)+{}^3G_5(15\%)+{}^3F_4(10\%)+{}^1G_4(8\%)+{}^1H_5(5\%)$
43	41175	$^3G_5(44\%)+{}^1P_1(26\%)+{}^3H_5(12\%)+{}^3G_5(8\%)$
45	46712	$^3D_1(39\%)+{}^3H_4(30\%)+{}^3P_1(16\%)+{}^1G_4(6\%)$
50	48251	$^3H_5(26\%)+{}^1H_5(24\%)+{}^3G_3(22\%)+{}^1F_3(10\%)+{}^1P_1(6\%)$
51	48533	$^1P_1(44\%)+{}^1H_5(22\%)+{}^3H_5(17\%)+{}^3D_1(8\%)$
57	50390	$^3G_4(49\%)+{}^1G_4(28\%)+{}^3D_1(7\%)+{}^1G_4(6\%)$

for the Coulomb interaction parameters $G^1(fd)$ and $G_5(fd)$ each produces fairly linearly decreasing energies for the levels below 27 700 cm^{-1}. The exceptions to this are two T_{1u} levels which exhibit a very different behavior, with one increasing (No. 4) and one decreasing (No. 7) nonlinearly (not fully shown in Fig. 6). A decrease of $G^1(fd)$ by ~270 cm^{-1} (dashed dot line in Fig. 6) or of $G^5(fd)$ by ~1000 cm^{-1} (not shown in Fig. 6) can bring the splitting between T_{2u} (No. 3) and T_{1u} (No. 4) to 7 cm^{-1}. The change in $G^1(fd)$ or (especially the much bigger change) in $G^5(fd)$ not only changes the positions of other levels quite a lot, but also changes the intensity ratios between different absorption peaks and, hence, was not used in the final calculation. All the No. 3–8 levels depend very weakly on $G^3(fd)$ in the same way. With $F^2(fd)$ and $F^4(fd)$ increasing from their optimized values (Table II), the lowest T_{1u} (No. 4) moves downward to approach the T_{2u} (No. 3) gradually, but the amount of change required is so big that positions of other much higher energy levels and the relative absorption intensities change thoroughly. To summarize this discussion of permissible parameter variations, we find that the lowest energy emission band at room temperature cannot originate from a T_{1u} level, but the higher energy emission band originates from the lowest T_{1u} level. The requirement of a T_{2u} level underlying T_{1u} by 7 cm^{-1} together with a gap of >1000 cm^{-1} (i.e., ~5 phonons) between this T_{2u} and the next lower level places strict constraints on the interaction parameters, in that they can only vary in a very small range and some of them can only vary simultaneously in constrained ways. In contrast to previous calculations,[6,7] the parameters were optimized in our calculation to get a better overall agreement between the calculated and measured energy levels. The Coulomb interaction parameters turned out to be reduced greatly from the free ion values, similar to the case reported for $SrCl_2:Tm^{2+}$ (Ref. 8) and the recent results on trivalent lanthanide ions.[54] The calculation presented here also shows that Coulomb interaction plays an important role and cannot be neglected in the analyses of the $4f^{N-1}5d$ energy level structure, and the introduction of different types of Yb^{3+} sites[7] is not necessary to explain the complexity of the $4f^{14}-4f^{13}5d$ spectrum of Yb^{2+}, since all the absorption peaks appear naturally in the calculated spectra.

3. Oscillator strengths, g values, and interacting configuration

The parameter values (Table II) and calculated energy levels (Table I, column 6) presented here can also be justified by the calculated relative oscillator strengths in the absorption spectrum (Table I, column 10), the emission spectra, and the lifetime measurements (Sec. III D). The *SLJ* (*S, L, J,* being total spin, total orbit, and total angular momenta quantum numbers, respectively), multiplet term parentages of certain energy levels including the eight lowest and seven (extra) levels with strong absorption are listed in Table III. It is evident that the lowest two levels (1: E_u and 2: T_{2u}) are not only almost pure triplets, but their transitions to the electronic ground state are also symmetry forbidden. There are

many states (for example, levels 3: T_{2u} and 6: E_u) with substantial singlet components, but the respective transitions are also symmetry forbidden. Only one terminal level (51: T_{1u}) of the allowed absorption transitions involves a state dominated by singlet components, showing that spin mixing is strong.

We have also fine-tuned the calculation by consideration of two other factors. First, Kaplyanskii *et al.*[50] have measured the g factors of the emissive T_{1u} (27 049 cm^{-1}) and T_{2u} (27 042 cm^{-1}) states as 1.78 ± 0.07 and -0.7 ± 0.2, respectively. Our calculated values were $g(T_{1u})=2.3$ and $g(T_{2u})=-0.86$. However, the next highest T_{1u} level calculated at 27 572 cm^{-1} has a smaller g value of 1.4, and the smaller separation and greater extent of mixing with the lowest T_{1u} tend to reduce the g value of the latter state. Second, we have noticed that experiments show that for the free Yb^{2+} ion, the $4f^{13}6s^1$ configuration occurs at relatively low energy.[59] There are four levels of the free ion from this configuration: at 34 656, 34 990, 44 854, and 45 208cm^{-1}. The gap between the first two and the second two levels is due to $H_{so}(f)$, and the gap between levels 1 and 2, or between levels 3 and 4, is due to the exchange interaction between $4f$ and $6s$ orbitals. Absorption from $4f^{14}$ to $4f^{13}6s$ states is electric dipole forbidden, but this selection rule can be lifted by combining the mixing between $4f^{13}6s$ and $4f^{13}5d$ due to interaction between those two configurations [Coulomb interaction described by $R^2(4f4f,5d6s)=-188$ cm^{-1} and $R^3(5d4f,4f6s)=2309$ cm^{-1}] and the mixing of different terms in $4f^{13}5d$. The configuration interaction can shift $4f^{13}6s$ levels and those nearby $4f^{13}5d$ levels by energies up to the order of 100 cm^{-1} depending on the separation between those levels when this interaction is turned off, but it has negligible impact on other $4f^{13}5d$ levels. The s-character levels may have a larger coupling with the lattice and, hence, a larger Stokes shift. The levels at 34 656 cm^{-1} ($J=4$) and 44 854 cm^{-1} ($J=2$) are purely spin $S=1$ states and, hence, exhibit spin-forbidden transitions. By comparison, the levels at 34 990 cm^{-1} ($J=3$) and 45 208 cm^{-1} ($J=3$) contain roughly half $S=1$ and half $S=0$ components and, hence, exhibit spin-allowed transitions. The $J=3$ multiplet reduces to $T_{2u}+T_{1u}+A_{1u}$ at the O_h site and, hence, transitions are also orbit allowed. The $4f^{13}6s^1$ states are not subject to the large crystal field splitting experienced by $4f^{13}5d^1$. The experimentally located 35 028 and 45 794 cm^{-1} levels for Yb^{2+} in $SrCl_2$ here are then assigned to the two T_{1u} levels from $4f^{13}6s^1$ rather than from $4f^{13}5d^1$, with both the right positions and weak transition intensities. By treating those two troublesome levels as $4f^{13}6s^1$, the rms of fitting the remaining 12 levels [using only the parameters $F^2(fd)$, $G^1(fd)$, $B_0^4(dd)$, and E_{exc}] was greatly reduced from ~300 to ~100 cm^{-1}, which is in the region of experimental precision. The parameters (Table I) and energy levels (Table II) were then almost the same as those in the calculation without taking those two levels into account, and the fitting of intensities was slightly improved.

D. Spectral intensity and lifetime of emission of $SrCl_2:Yb^{2+}$

The following discussion focuses on the nominal 0.05 at. % Yb^{2+} doped sample of $SrCl_2$. The measured emission spectra are characterized by two peaks separated from each other by ~1800 cm^{-1} at room temperature (Fig. 3), and the lifetimes of the higher and lower energy peaks are a few tenths of a microsecond and a millisecond, respectively. These facts can be well explained by the calculated energy levels and dipole strengths reported here. Our three-level theoretical model using Table I for considering the emission spectra is shown diagrammatically in Fig. 7. The transition from level 4 is electric dipole allowed. The transition from level 3: T_{2u} (experimentally at 7 cm^{-1} lower in energy than the T_{1u} state) is electric dipole forbidden but electric dipole vibronic allowed by coupling to certain non-totally-symmetric even parity phonons. The energy levels 3–8 (Table I: termed group A) are close and the approximation of thermal equilibrium among them is reasonable, just as for energy levels 1 and 2 (termed group B) calculated to be 4 cm^{-1} apart with similar degeneracy-weighted occupancy. The direct electric dipole transition from energy levels 1 and 2 of $4f^{13}$ $5d$ to the $4f^{14}$ ground state is forbidden due to O_h symmetry selection rule, but it is weakly allowed by the assistance of appropriate phonons. The radiative lifetime is expected to be near the millisecond range and we take the measured value at 300 K of 0.598 ms of the peak centered at 395–425 nm. The calculated gap (1920 cm^{-1}) between levels 2 and 3 is bridged by about ten phonons.

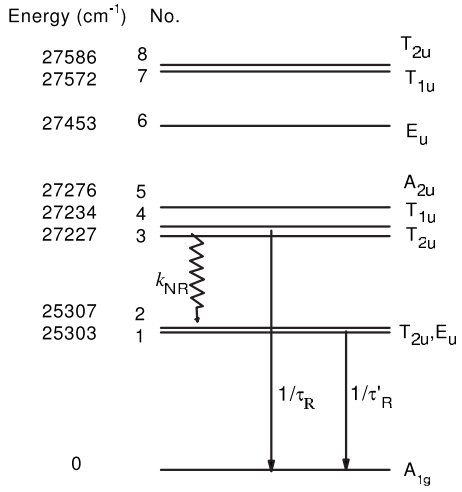

FIG. 7. Model for calculating emission relative intensities and lifetimes.

The temperature dependence of the measured emission lifetime, τ_R(expt), and calculated radiative lifetime, τ_R(calc), of the peak between 370 and 390 nm (band I) are listed in columns 2 and 3 of Table IV. The measured lifetime can be considered as solely due to radiative emission at temperature <240 K. The decrease of the measured lifetime from 250 to 300 K is attributed to nonradiative depopulation, which becomes much slower at lower temperatures when only levels 3 and 4 are appreciably populated. The theoretical lifetime, τ_R(calc), is calculated by assuming thermal equilibrium among the energy levels above 27 000 cm^{-1}:

TABLE IV. Temperature dependence of the lifetime τ(expt) of band I at 370–390 nm, the calculated radiative lifetime τ_R(calc), nonradiative depopulation rate k_{NR}(calc), and intensity ratio of band II /band I, R(calc). Data for R(calc) in brackets are deduced from the measured intensity ratio by normalizing the ratio at 300 K to the average value 1 (from different measurements, see text) and data for k_{NR}(calc) in brackets are calculated using k_{NR}(calc) $=R$(calc)$/\tau_R$(calc).

T (K)	τ(expt) (μs)	τ_R(calc) (μs)	k_{NR}(calc) (10^6 s^{-1})	R(calc)
300	0.55	0.86	0.65	0.55
290	0.62	0.85	0.43	0.37
280	0.68	0.84	0.28	0.24
270	0.71	0.83	0.21	0.17
260	0.75	0.82	0.12	0.10
250	0.75	0.82	0.11	0.09
240	0.82	0.81		
230	0.78	0.80	(0.025)	(0.020)
220	0.75	0.79	(0.018)	(0.014)
200	0.76	0.77	(0.013)	(0.010)
150	0.72	0.73	(0.011)	(0.008)
100	0.7	0.70	(0.013)	(0.009)
50	0.73	0.70	(0.010)	(0.007)
10	1.04	1.13	(0.009)	(0.010)

$$\frac{1}{\tau_R(\text{calc})} = \frac{\sum_{i=3,\ldots,8} g_i \gamma_i \exp\left(-\frac{\Delta E_i}{k_B T}\right)}{\sum_{i=3,\ldots,8} g_i \exp\left(-\frac{\Delta E_i}{k_B T}\right)}, \quad (1)$$

where g_i is the degeneracy of energy level i; γ_i is the spontaneous emission rate for energy level i; and ΔE_i is the relative position of energy level i. Now $\Delta E_3 = -7$ cm^{-1} (relative to level 4) and $\Delta E_4 = 0$ cm^{-1} (reference level) and the calculated energies are used to derive ΔE_{5-8}. The spontaneous emission rate from the initial energy level I (with partner denoted as b) to final energy level F (with partner denoted as a, just one state $|f^{14}\,{}^1S_0\rangle$) is

$$\gamma_{I\to F} = \frac{1}{4\pi\varepsilon_0}\frac{4\omega^3}{3\hbar c^3} n_R f_{\text{local}}^2 \frac{e^2\langle d|r|f\rangle^2}{g_I} \sum_{qab} |\langle Fa|C_q|Ib\rangle|^2, \quad (2)$$

where $n_R = 1.69$ (Ref. 60) is the refractive index for the appropriate photon energy; g_I is the degeneracy of the initial level of the transition; $\langle 5d|r|4f\rangle$ is an effective radial integral with the configuration interaction (CI) effect taken into account, with the Hartree-Fock value (without taking CI effect into account) being 0.0324 nm,[61] many-body perturbation theory value (with the most important CI effects) being 0.0253 nm,[62] and experimental value fitted from the $T < 240$ K measured lifetime being 0.0228 nm; and f_{local} is the ratio of the local radiation field to the macroscopic radiation field (calculated microscopically[62] to be 1.5), which deviates from the Lorentz model $(n_R^2+2)/3 = 1.62$, due to the fact that the polarization factor for Sr^{2+} is not negligibly small but about half of that for Cl^-.[60] The calculated radiative lifetime is plotted as a function of temperature in Fig. 8. It decreases slightly from room temperature (0.86 μs) to 50 K (0.70 μs) and then increases down to 10 K (1.13 μs). The calculated nonradiative rate k_{NR}(calc) of the 370–390 nm (group A) emission levels to the emission levels centered at 410 nm (group B) for $T \geqslant 250$ K is given by

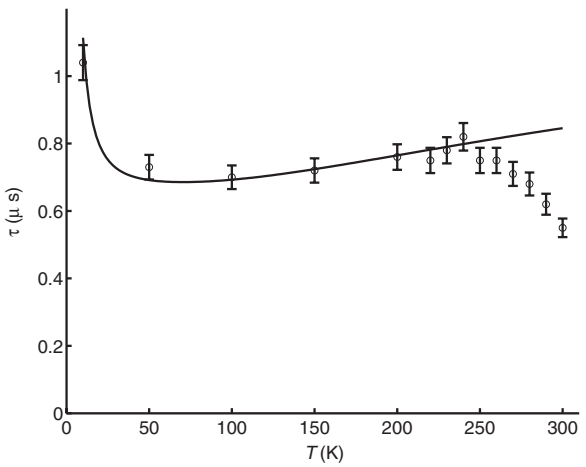

FIG. 8. Measured lifetime (circle with 5% error bar) and calculated radiative lifetime (line) of the peak between 370 and 390 nm in $SrCl_2:Yb^{2+}$.

$$k_{NR} = 1/\tau(\text{expt}) - 1/\tau_R(\text{calc}), \quad (3)$$

and is listed in column 4 of Table IV. The rate decreases substantially between room temperature and 250 K.

The intensity ratio at room temperature of band II/band I was found to vary with the excitation wavelength of the spectrofluorometer, being 0.8 for 304 nm excitation and 1.1 for 355 nm excitation. The room temperature 334 nm excited spectrum of Witzke *et al.*[31] exhibits a ratio of 0.96. This intensity ratio R not only depends on excitation wavelength but also on Yb^{2+} concentration,[31] and these factors are attributed to changes in self-absorption and energy level nonradiative bypassing mechanisms. A linear fit is obtained from the plot of the natural logarithm of the intensity ratio ($\ln R$) versus reciprocal temperature in the range from room temperature to 250 K in Fig. 9(a). Such a strong temperature dependent nonradiative relaxation cannot be described by the direct multiphonon relaxation process. The energy gap $\sim$2000 cm^{-1} corresponds to only 9–10 phonons of energy about 213 cm^{-1}. Calculations based on Kiel's multiphonon emission formula[65] or other variations result in $k_{NR}(300)/k_{NR}(250) \sim 2.7$, while the experimental $k_{NR}(300)/k_{NR}(250) \sim 6$ requires a 20 phonon process. Below $\sim$250 K, the nonradiative relaxation rate is very small for populating group B levels and our spectra are confused by the appearance of Eu^{2+} emission. The relative intensity ratio R in the regime below 230 K is shown in Fig. 9(b). We have calculated the intensity ratio by the equation

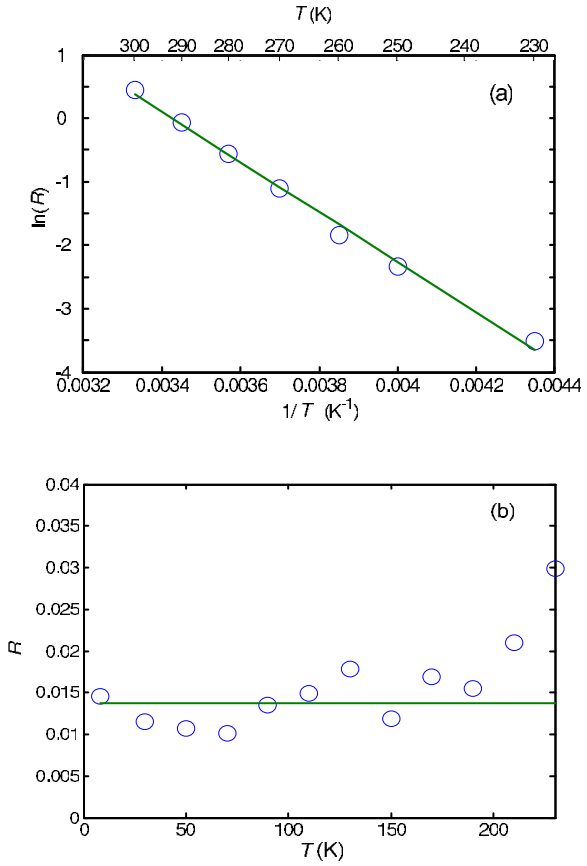

FIG. 9. (Color online) Intensity ratio R of band I/band II emission peaks as a function of temperature: (a) $\ln(R)$ vs $1/T$ for $T \geqslant 250$ K and (b) R vs T for $T \leqslant 230$ K. The linear fit to (a) is $\ln(R) = 13.5 \pm 0.5 - (3954 \pm 135)T^{-1}$. The mean value below 200 K in (b) is 0.014.

$$R(\text{calc}) = k_{\text{NR}}(\text{calc})\,\tau_R(\text{calc}) \tag{4}$$

and this is tabulated in column 5 of Table IV and is somewhat smaller than the measured intensity ratio. The nonradiative relaxation rate, $k_{\text{NR}}(T)$, from group A to group B levels can be written as a function of temperature using the strong coupling rate equation[63,64]:

$$k_{\text{NR}}(T) = k_{\text{NR}}(0) + A \exp\left(-\frac{\Delta E}{k_B T}\right). \tag{5}$$

where ΔE is an energy parameter and A is a frequency factor. The backward thermal excitation from group B to group A is $\exp[(E_B - E_A)/k_B T]$ times $k_{\text{NR}}(T)$ and is negligible. By using the value of ΔE (3954 K, 2744 cm^{-1}) from the slope of Fig. 9(a), the temperature dependence of the nonradiative rate from group A can be well fitted to the values in column 4 of Table IV by Eq. (5), as shown in Fig. 10. The parameters $k_{\text{NR}}(0)$ and A are optimized to be 1.06×10^4 and 4.0×10^{11} s^{-1}, respectively.

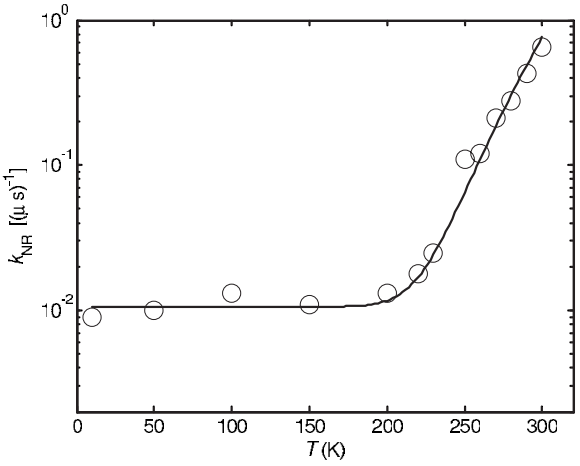

FIG. 10. Dependence of the nonradiative relaxation rate $k_{\text{NR}}(T)$ (Table IV, column 4) on temperature T. The fit by Eq. (5) using $\Delta E = 2944$ cm^{-1} gives $k_{\text{NR}}(0) = 1.06 \times 10^4$ s^{-1} and $A = 4.0 \times 10^{11}$ s^{-1}.

IV. CONCLUSIONS

The main conclusions from this study are itemized below.

(1) The derived energy levels from the electronic absorption spectrum of Yb^{2+} situated at a site of cubic symmetry in $SrCl_2$ have been fitted by a $4f^{13}\,5d$ crystal field calculation and the calculated oscillator strengths are in reasonable agreement with experiment. The energy parameters are in agreement with those from other studies of the electronic spectra of dipositive lanthanide ions.

(2) The room temperature emission spectrum of $SrCl_2:Yb^{2+}$ comprises two broad bands, with lifetimes in the micro- and millisecond ranges. Both transitions are formally spin forbidden. The higher energy transition is orbitally allowed, whereas the lower energy band is orbitally forbidden. The calculated radiative lifetime for the higher energy transition (~ 1 μs) is in agreement with that measured at 10 K.

(3) The temperature-intensity dependence of the two bands and the lifetime of the higher energy emission have been modeled by a three-level system. The lifetime varies with temperature mainly because (i) the luminescent level is in thermal equilibrium with other levels which have forbidden transitions, and, (ii) at higher temperatures ($T > 240$ K), the nonradiative relaxation to lower levels at ~ 1900 cm^{-1} below is appreciable. The temperature dependence of the nonradiative relaxation rate is well simulated by calculation.

(4) As in previous studies, our experiments were complicated by the presence of impurities in our samples. This did not enable us to study the low energy emission band at low temperatures.

ACKNOWLEDGMENTS

This work was supported by the Hong Kong Research Grants Council CERG grant CityU 102607. C.-K.D. acknowledges financial support for this study under the City University Research Grant 9360123.

*Permanent address: Chongqing University of Posts and Telecommunications, Chongqing 400065, People's Republic of China.
[1] J. Rubio O, J. Phys. Chem. Solids **52**, 101 (1991).
[2] W. E. Bron and M. Wagner, Phys. Rev. **139**, A233 (1965).
[3] M. Wagner and W. E. Bron, Phys. Rev. **139**, A223 (1965).
[4] J. D. Axe and P. P. Sorokin, Phys. Rev. **130**, 945 (1963).
[5] W. E. Bron and W. R. Heller, Phys. Rev. **136**, A1433 (1964).
[6] T. S. Piper, J. P. Brown, and D. S. McClure, J. Chem. Phys. **46**, 1353 (1967).
[7] E. Loh, Phys. Rev. B **7**, 1846 (1973).
[8] R. C. Alig, R. C. Duncan, and B. J. Mokross, J. Chem. Phys. **59**, 5837 (1973).
[9] S. W. Bland and M. J. A. Smith, J. Phys. C **18**, 1525 (1985).
[10] S. Schweizer, Phys. Status Solidi A **187**, 335 (2001).
[11] C. Wickleder, J. Lumin. **94-95**, 127 (2001).
[12] H. Hagemann, F. Kubel, H. Bill, and F. Gingl, J. Alloys Compd. **374**, 194 (2004).
[13] Z.-Y. He, Y.-S. Wang, S. Li, and X.-R. Xu, J. Lumin. **97**, 102 (2002).
[14] W. Zhang, H. J. Seo, B. K. Moon, S.-S. Yi, and K. Jang, J. Alloys Compd. **374**, 32 (2004).
[15] Q. Su, H. Liang, T. Hu, Y. Tao, and T. Liu, J. Alloys Compd. **344**, 132 (2002).
[16] Z. Lian, J. Wang, Y. Lv, S. Wang, and Q. Su, J. Alloys Compd. **430**, 257 (2007).
[17] X. Zhang, J. Zhang, J. Xu, and Q. Su, J. Alloys Compd. **389**, 247 (2005).
[18] Z. Fu, S. Zhou, Y. Yu, and S. Zhang, Chem. Phys. Lett. **395**, 285 (2004).
[19] C. K. Duan, M. F. Reid, and G. W. Burdick, Phys. Rev. B **66**, 155108 (2002).
[20] C. K. Duan, A. Meijerink, R. J. Reeves, and M. F. Reid, J. Alloys Compd. **408**, 784 (2006).
[21] Z. Pan, L. Ning, B.-M. Cheng, and P. A. Tanner, Chem. Phys. Lett. **428**, 78 (2006).
[22] P. Dorenbos, J. Phys.: Condens. Matter **17**, 8103 (2005).
[23] P. Dorenbos, J. Lumin. **122-123**, 315 (2007).
[24] P. Dorenbos, J. Lumin. **104**, 239 (2003).
[25] P. Dorenbos, J. Phys.: Condens. Matter **15**, 4797 (2003).
[26] P. Dorenbos, J. Alloys Compd. **341**, 156 (2002).
[27] O. S. Wenger, C. Wickleder, K. W. Krämer, and H. U. Güdel, J. Lumin. **94-95**, 101 (2001).
[28] J. Grimm, J. F. Suyver, E. Beurer, G. Carver, and H. U. Güdel, J. Phys. Chem. B **110**, 2093 (2006).
[29] J. Grimm, O. S. Wenger, K. W. Krämer, and H. U. Güdel, J. Lumin. **126**, 590 (2007).
[30] S. M. Kaczmarek, T. Tsuboi, M. Ito, G. Boulon, and G. Leniec, J. Phys.: Condens. Matter **17**, 3771 (2005).
[31] H. Witzke, D. S. McClure, and B. Mitchell, in *Luminescence of Crystals, Molecules and Solutions*, edited by F. E. Williams (Plenum, New York, 1973), p. 598.
[32] S. Lizzo, A. Meijerink, G. J. Dirksen, and G. Blasse, J. Lumin. **63**, 223 (1995).
[33] L. Su, J. Xu, H. Li, L. Wen, W. Yang, Z. Zhao, J. Si, Y. Dong, and G. Zhou, J. Cryst. Growth **277**, 264 (2005).
[34] L. Su, J. Xu, H. Li, L. Wen, Y. Zhu, Z. Zhao, Y. Dong, G. Zhou, and J. Si, Chem. Phys. Lett. **406**, 254 (2005).
[35] M. Henke, J. Persson, and S. Kück, J. Lumin. **87-89**, 1049 (2000).
[36] M. Nikl, A. Bensalah, E. Mihokova, J. Hybler, H. Sato, T. Fukuda, and G. Boulon, Opt. Mater. (Amsterdam, Neth.) **24**, 191 (2003).
[37] S. Lizzo, A. Meijerink, and G. Blasse, J. Lumin. **59**, 185 (1994).
[38] X. Zhao, Y. Deng, Z. Li, and S. Wang, J. Alloys Compd. **250**, 405 (1997).
[39] C. P. An, V. Dierolf, and F. Luty, Phys. Rev. B **61**, 6565 (2000).
[40] S. Lizzo, E. P. K. Nagelvoort, R. Erens, A. Meijerink, and G. Blasse, J. Phys. Chem. Solids **58**, 963 (1997).
[41] P. Dorenbos, J. Phys.: Condens. Matter **15**, 2645 (2003).
[42] R. T. Wegh and A. Meijerink, Phys. Rev. B **60**, 10820 (1999).
[43] C. Ma, P. A. Tanner, S. Xia, and M. Yin, Opt. Mater. (Amsterdam, Neth.) **29**, 1620 (2007).
[44] P. Dorenbos, J. Phys.: Condens. Matter **15**, 575 (2003).
[45] P. Larsen, M. Adlung, and C. Wickleder, Rare Earth Conference, Wroclaw, 2006 (unpublished), Abstract CI3.
[46] P. W. M. Jacobs and M. L. Vernon, Can. J. Chem. **76**, 1540 (1998).
[47] P. A. Tanner, Top. Curr. Chem. **241**, 167 (2004).
[48] H. Witzke, D. S. McClure, and B. Mitchell, Izv. Akad. Nauk SSSR, Ser. Fiz. **37**, 705 (1973).
[49] A. A. Kaplyanskii and P. L. Smolyanskii, Sov. Phys. Solid State **17**, 357 (1975).
[50] A. A. Kaplyanskii, P. L. Smolyanskii, and I. N. Uraltsev, Fiz. Tverd. Tela (Leningrad) **17**, 1816 (1975).
[51] A. A. Kaplyanskii and P. L. Smolyanskii, Opt. Spektrosk. **40**, 528 (1976).
[52] H. Yersin, H. Otto, J. I. Zink, and G. Gliemann, J. Am. Chem. Soc. **102**, 951 (1980).
[53] M. F. Reid, L. van Pieterson, R. T. Wegh, and A. Meijerink, Phys. Rev. B **62**, 14744 (2000).
[54] L. van Pieterson, M. F. Reid, G. W. Burdick, and A. Meijerink, Phys. Rev. B **65**, 045114 (2002).
[55] H. A. Weakliem and Z. J. Kiss, Phys. Rev. **157**, 277 (1967).
[56] M. J. Weber and R. W. Bierig, Phys. Rev.. **134**, A1492 (1964).
[57] We are indebted to Lixin Ning for performing this calculation.
[58] M. C. Downer, C. D. Cordero-Montalvo, and H. Crosswhite, Phys. Rev. B **28**, 4931 (1983).
[59] K. J. Öberg and H. Lundberg, Eur. Phys. J. D **42**, 15 (2007).
[60] K. Shirao, Y. Fujii, J. Tominaga, K. Fukushima, and Y. Iwadate, J. Alloys Compd. **339**, 309 (2002).
[61] T. Chen, C.-K. Duan, and S. D. Xia, J. Alloys Compd. **439**, 363 (2007).
[62] C.-K. Duan, L. G. Chen, and M. F. Reid, Curr. Appl. Phys. (to be published).
[63] N. F. Mott, Proc. R. Soc. London, Ser. A **A167**, 384 (1938).
[64] R. Englman and J. Jortner, Mol. Phys. **18**, 145 (1970).
[65] T. Tsuboi, H. Witzke, and D. S. McClure, J. Lumin. **24/25**, 305 (1981).